

# Nanoscale

Accepted Manuscript



This is an *Accepted Manuscript*, which has been through the Royal Society of Chemistry peer review process and has been accepted for publication.

*Accepted Manuscripts* are published online shortly after acceptance, before technical editing, formatting and proof reading. Using this free service, authors can make their results available to the community, in citable form, before we publish the edited article. We will replace this *Accepted Manuscript* with the edited and formatted *Advance Article* as soon as it is available.

You can find more information about *Accepted Manuscripts* in the [Information for Authors](#).

Please note that technical editing may introduce minor changes to the text and/or graphics, which may alter content. The journal's standard [Terms & Conditions](#) and the [Ethical guidelines](#) still apply. In no event shall the Royal Society of Chemistry be held responsible for any errors or omissions in this *Accepted Manuscript* or any consequences arising from the use of any information it contains.

## COMMUNICATION

## Flexible Prototype Thermoelectric Devices Based on Ag<sub>2</sub>Te and PEDOT:PSS Coated Nylon Fibre

Cite this: DOI: 10.1039/x0xx00000x

Scott W. Finefrock,<sup>a</sup> Xiaoqin Zhu,<sup>a</sup> Yanming Sun,<sup>ab</sup> and Yue Wu<sup>c,\*</sup>

Received 00th January 2012,  
Accepted 00th January 2012

DOI: 10.1039/x0xx00000x

[www.rsc.org/](http://www.rsc.org/)

**p- and n- type Ag<sub>2</sub>Te nanocrystals are coated separately onto nylon fibres to create flexible composites. A prototype thermoelectric device made using such fibres produces ~0.8 nW in a 20 K temperature difference. This is improved to over 5 nW by using a conducting polymer as the p-type material.**

Thermoelectric devices are heat engines that are used in several niche applications such as small scale refrigeration, electricity co-generation, remote power generation, and waste heat recovery.<sup>1-6</sup> The devices operate based on the Seebeck and Peltier effects and are comprised of p- and n-type semiconductors. Device efficiency scales with the figure of merit,  $ZT = S^2\sigma T/\kappa$  where  $S$  is the Seebeck coefficient,  $\sigma$  is electrical conductivity,  $\kappa$  is thermal conductivity, and  $T$  is absolute temperature.<sup>1,3,6</sup> Lately, there has been much interest in broadening the use of thermoelectric technology to applications that require or could benefit from flexibility.<sup>7-9</sup>

A few classes of flexible thermoelectric materials have been developed, including polymer/telluride composites,<sup>10-16</sup> polymer/carbon nanotube composites,<sup>17-26</sup> polymer/graphene composites,<sup>27,28</sup> and telluride coated fibres.<sup>29,30</sup> In several cases, researchers have made and characterized the power output of prototype devices.<sup>30-34</sup> One issue in this research area is the scarcity of air-stable n-type materials. Our lab made a breakthrough in developing n-type PbTe nanocrystals doped with iodine and has successfully demonstrated the functional prototype thermoelectric energy harvesting device fabricated on PbTe nanocrystals coated glass fibres and substrates.<sup>31,35</sup> One issue with these PbTe nanocrystal-based devices is the need for a high temperature (300-350 °C) annealing step, which prevents the use of low-cost polymeric fibre substrates

such as nylon, polyester, or cotton. Both of the issues in this research area are addressed by the present development of a new material, Ag<sub>2</sub>Te nanocrystal coated nylon fibres.

The use of Ag<sub>2</sub>Te is motivated by several factors. First, colloidal nanocrystals of Ag<sub>2</sub>Te can be synthesized in a scalable way using established procedures.<sup>36-39</sup> Second, Ag<sub>2</sub>Te is known to have moderate ZT values near room temperature.<sup>40,41</sup> Third, Ag<sub>2</sub>Te nanocrystal films have high electrical conductivities even prior to heat treatment.<sup>42</sup> Fourth, the type of carrier can sometimes be changed by adjusting the synthesis precursor ratios.<sup>43</sup>

Ag<sub>2</sub>Te nanocrystals are synthesized in solution, washed, and coated onto nylon fibre mesh by a successive dip-coating approach. For the synthesis, a modified version of the method described previously is used.<sup>37</sup> Solution A is made by dissolving 1.28 ml 1-dodecanethiol in 80 ml 4-tertbutyltoluene. Solution B is made by dissolving 0.364 g AgNO<sub>3</sub> in 80 ml deionized water using sonication. Solution B is then added to solution A and the mixture is stirred for 2-3 hours. A stock Te precursor solution is made in a nitrogen filled glove box by dissolving 4.79 g Te powder in 50 ml triocetylphosphine (TOP) by stirring on a 60 °C hot plate. The white organic phase of the Ag precursor solution is transferred to a 100 ml 3-neck flask using a separator funnel. Nitrogen gas protection is applied using a Schlenk line and the solution is heated to approximately 97 °C at which point 3 ml of the TOP-Te solution are rapidly injected. The reaction temperature is kept at 97 °C for 24 hours and is then quenched to room temperature using a water bath.

The reaction products are combined with 8 ml hexane and centrifuged briefly at 4300 rpm. The supernatant is combined with an equal volume of ethanol and centrifuged at 6000 rpm.

The resulting precipitate is dissolved in hexane and centrifuged at 4000 rpm. The resulting supernatant is combined with ethanol and centrifuged to obtain a precipitate that is dissolved in 10 ml chloroform in preparation for dip coating onto nylon.

The nanocrystals are characterized using powder X-ray diffraction (XRD) and transmission electron microscopy (TEM). The XRD pattern of nanocrystals dip coated onto glass in Figure 1a shows that the material is pure hessite  $\text{Ag}_2\text{Te}$ . The low magnification TEM image in Figure 1b shows that the nanocrystals have typical size of  $10 \pm 2$  nm, although larger nanocrystals can also occasionally be seen. The high resolution TEM image in Figure 1c shows the lattice-resolved image of several single crystalline nanocrystals.

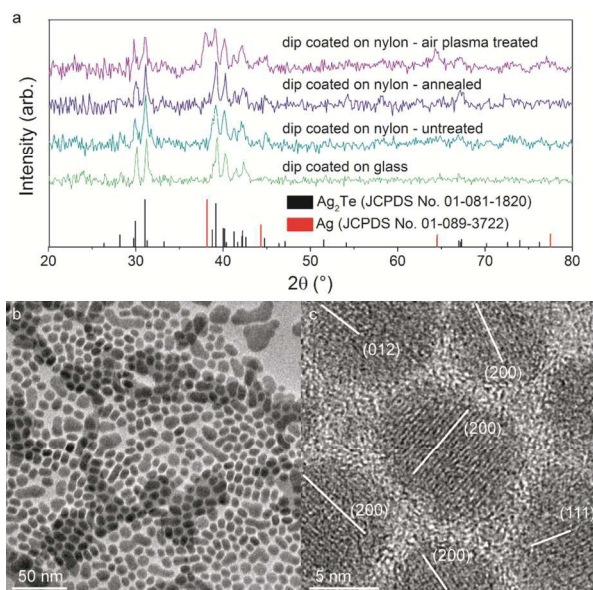
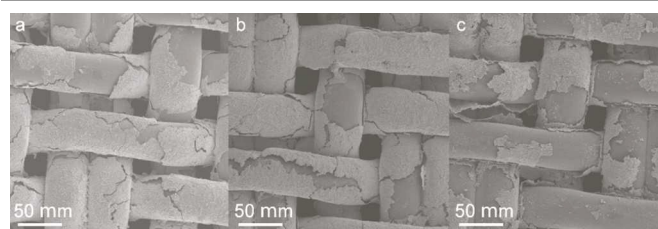


Figure 1. (a) XRD pattern of  $\text{Ag}_2\text{Te}$  nanocrystals and  $\text{Ag}_2\text{Te}$  coated nylon. (b) Low magnification image of  $\text{Ag}_2\text{Te}$  nanocrystals. (c) High resolution image of  $\text{Ag}_2\text{Te}$  nanocrystals.

Nylon mesh is prepared for dip coating by sonication in a 50/50 (v/v) solution of isopropanol and acetone followed by drying in an oven at 80 °C and finally by treating in an air plasma cleaner for 30 minutes. The nanocrystals are coated onto nylon fibre mesh using a modified version of the technique described previously.<sup>29</sup> In the present three-step dip-coating procedure, the first solution is one batch of  $\text{Ag}_2\text{Te}$  nanocrystals dissolved in 10 ml chloroform, the second solution is 0.048 M  $\text{N}_2\text{H}_4$  in ethanol, and the third solution is ethanol. As shown in Figure S1, the coated nylon mesh possesses a measurable electrical conductance after only 30 dip coating cycles regardless of the nanocrystal size distribution. However, 50 coating cycles using nanocrystals with sizes similar to those in Figure 1b possess the lowest measured sheet resistances. Therefore, all subsequent results are obtained using similarly made low resistance material.

To investigate potential enhancement of the thermoelectric properties of  $\text{Ag}_2\text{Te}$  nanocrystal coated nylon, two treatment methods are employed. In the first method, the coated fibres

are annealed in a tube furnace at a pressure of approximately one torr at 127 °C for 30 minutes. This annealing treatment is motivated by the improvement observed after annealing similar materials.<sup>29,44</sup> In the second method, the coated fibres are treated in an air plasma cleaner for 10 minutes. This air plasma treatment is motivated by the significant impact such treatment has on many thin film materials.<sup>45-48</sup> The effect of the treatment methods on the structure of the coated nylon is shown in the SEM images in Figure 2a-c. Cracks in the coating and regions of bare nylon are observed even in the untreated material (Figure 2a), yet these features are even more pronounced in the annealed material (Figure 2b) and more so in the air plasma treated material (Figure 2c). The atomic ratio of Ag to Te is measured using energy dispersive X-ray spectroscopy (EDS) As shown in Figure 2d, the atomic ratios are very nearly equal to 2 for the untreated and annealed samples, as expected for  $\text{Ag}_2\text{Te}$ . The XRD patterns for these samples in Figure 1a further confirm the single-phase nature of the coating. The atomic ratio for the air plasma treated sample is nearly equal to 4. According to the published data on the Ag-Te system, such a composition at room temperature exists in the two-phase Ag- $\text{Ag}_2\text{Te}$  region of the phase diagram.<sup>49</sup> Accordingly, the XRD pattern (top spectrum, Figure 1a) for the air plasma treated sample possesses peaks from the (111) and (220) planes of Ag in addition to peaks from  $\text{Ag}_2\text{Te}$ . As there is no Ag source during the air plasma treatment, the increase in the Ag:Te ratio is necessarily associated with a loss of Te. While the exact mechanism of the Te loss is unclear at this point, the air plasma appears to act as a selective etching process.<sup>50</sup>



Sample	$R_s$ (W/□)	$S$ (mV/K)	$S^2/R_s$ (mV/K) <sup>2</sup> /(W/□)	Ag:Te (at. ratio)
Untreated	$1100 \pm 300$	$-78 \pm 13$	$5.5 \pm 2.3$	$2.11 \pm 0.03$
Annealed	$550 \pm 150$	$72 \pm 4.5$	$9.5 \pm 2.8$	$2.08 \pm 0.01$
Air plasma	$5.5 \pm 1.5$	$-22 \pm 0.2$	$90 \pm 25$	$3.86 \pm 0.29$
PEDOT:PSS	$3.2 \pm 2.2$	$15 \pm 0.1$	$71 \pm 50$	N.A.

Figure 2. SEM images of  $\text{Ag}_2\text{Te}$  nanocrystal coated nylon. (a) Untreated. (b) Annealed. (c) Air plasma treated. (d) Electrical properties and composition of coated nylon samples.

The room temperature electrical properties of the  $\text{Ag}_2\text{Te}$  nanocrystal coated nylon fibres are shown in Figure 2d. While it is preferable to measure the electrical conductivity of thermoelectric materials, the complex geometry of the coated nylon makes such a measurement impractical for the present samples. Thus the sheet resistance ( $R_s$ ) is used for comparison here and studies involving simpler planar geometry that allow for  $\sigma$  determination and a more fair comparison of materials of different thicknesses are well underway.<sup>42</sup> Note that the

values of  $R_s$  for the annealed and air plasma treated materials are based on approximate ratios of values obtained before and after treatment. The Seebeck coefficient values shown here are measured using an MMR SB100 Seebeck measurement system and represent estimates. The details of the measurement method and results are given in the supporting information. The fourth column ( $S^2/R_s$ ) is a modification of the power factor ( $S^2\sigma$ ), which is inversely proportional to  $R_s$  for a given sample thickness. As the thermal conductivity measurement of even straight coated fibres is challenging,<sup>51</sup> the thermal conductivity of the interwoven coated nylon fibres is not measured in the present study.

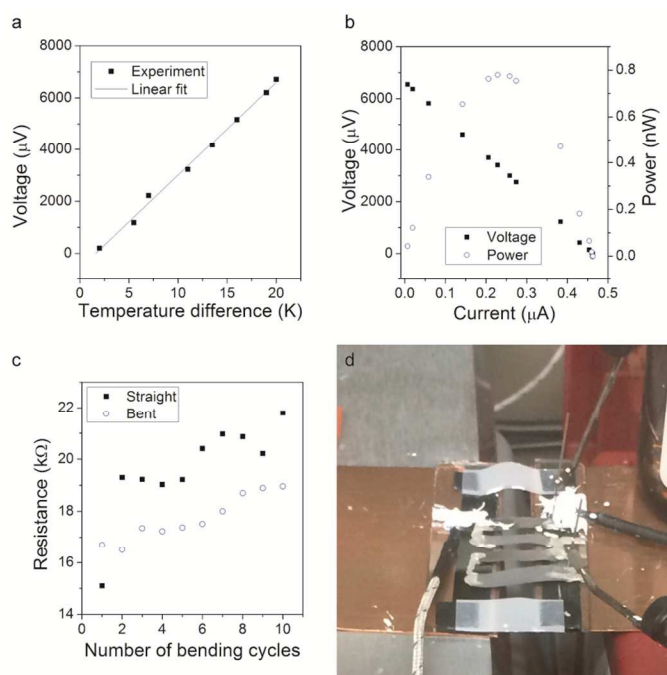
The untreated nanocrystals are n-type with Seebeck coefficients similar to those previously reported for  $\text{Ag}_2\text{Te}$  nanocrystal films.<sup>38</sup> After annealing, the coated nylon becomes p-type with a slight drop in Seebeck coefficient magnitude and a reduction in sheet resistance by a factor of two, which leads to an improved value of the modified power factor. The air plasma treated sample exhibits a drastically reduced Seebeck coefficient, yet the decrease in sheet resistance by over two orders of magnitude results in the largest value of the modified power factor observed in this study. These changes are likely due to the relatively low values for the Seebeck coefficient and electrical resistivity of Ag, which is present in the air plasma treated material.<sup>52,53</sup>

The annealed and air plasma treated material is used to make a four-leg prototype thermoelectric module, "device #1," shown in Figure 3d. Each leg is approximately 3 mm x 13 mm. The legs are glued to glass substrates and connected electrically using Ag paint at the two ends. The glass substrates are attached to copper fins using carbon tape. The bare nylon pieces at the top and bottom of the image lend the device additional mechanical support.

Figure 3. Characterization of device #1. (a) Open circuit voltage. (b) Voltage and power output in a temperature gradient of 20 K. (c) Device resistance during bending test. (d) Photograph of device during electrical characterization.

The device is characterized by placing one copper fin on a plastic stand and one fin on a hot plate that is used to create a temperature difference. Thermocouples are thermally bonded to the glass substrates on the hot and cold sides using silicone heat sink compound. Electrical connections to the device are made using microprobes. The open circuit voltage of the four-leg device in response to a temperature gradient is shown in Figure 3a. The slope of the best fit line is 356  $\mu\text{V}/\text{K}$ . While a 20 K temperature difference is sustained across the device, various load resistors are electrically connected. The current through and voltage across each resistor is measured and the power dissipated is calculated. The maximum power observed is just below 0.8 nW. Finally, the flexibility of the device is evaluated by measuring the resistance of the device in response to bending by pushing the copper fins closer together resulting in a bending radius of approximately 1-2 mm. As shown in Figure 3c, the resistance of the device increases by nearly 50 % after 10 bending cycles.

Regarding device #1, its main weaknesses are its high resistance, which is mostly due to the p-type legs, and its increase in resistance due to bending. To partially alleviate these weaknesses, poly(3,4-ethylenedioxythiophene):poly(styrenesulfonate) (PEDOT:PSS) coated onto nylon fibre mesh is explored as a candidate for the p-type legs. The coating is made using a similar method as those described previously.<sup>54,55</sup> A mixture of Clevis PH 1000 and 5 % (v/v) ethylene glycol is drop cast onto nylon mesh on a glass petri dish on a 150 °C hot plate. The material is allowed to dry at this temperature for 10 minutes after which the hot plate is cooled to room temperature. The electrical properties of the material are shown in Figure 2d and are superior to the annealed  $\text{Ag}_2\text{Te}$  nanocrystal coated nylon due to the decreased sheet resistance.



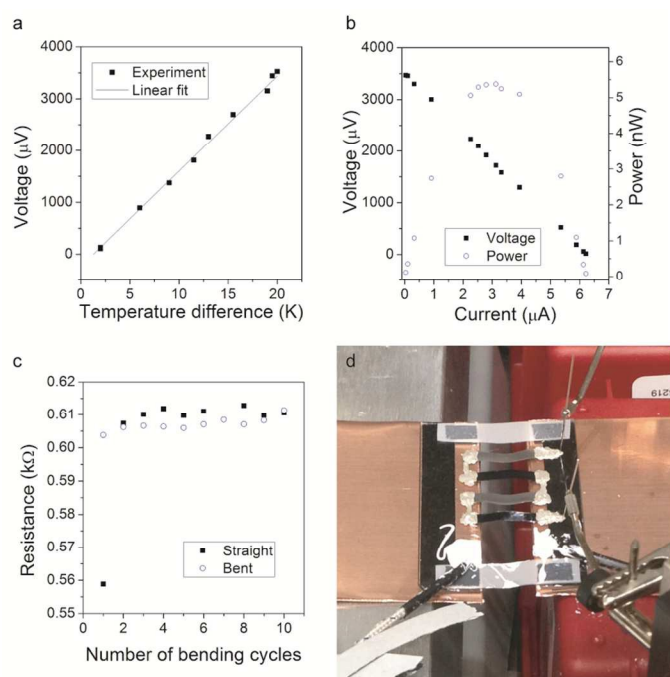


Figure 4. Characterization of device #2. (a) Open circuit voltage. (b) Voltage and power output in a temperature gradient of 20 K. (c) Device resistance during bending test. (d) Photograph of device during electrical characterization.

The four-leg prototype thermoelectric module, "device #2" made using p-type PEDOT:PSS coated nylon and n-type air plasma treated  $\text{Ag}_2\text{Te}$  nanocrystal coated nylon is shown in Figure 4d. The open circuit voltage (Figure 4a) has a best fit line with a slope of  $187 \mu\text{V}/\text{K}$ , which is nearly two times lower than that of device #1. However, the drastically reduced resistance results in a greatly increased power output of over 5 nW using a temperature difference of 20 K as shown in Figure 4b. Device #2 also fairs well during the bending test. Figure 4c shows how, after the first bending cycle, the device resistance increases by less than 2 % during the subsequent nine cycles.

Some examples of prior work involving prototype flexible thermoelectric devices do not include results for power output normalized by cross section area for heat flow, yet this quantity could be one useful figure of merit for such devices.<sup>33,34,56</sup> In the present work, the interwoven structure of the nylon makes exact determination of the cross section area difficult. Still, SEM images such as those in Figure 1 and other measurements suggest that the area normalized power outputs of device #1 and #2 from a temperature difference of 20 K are roughly 0.15 and 0.60  $\mu\text{W}/\text{cm}^2$ . These values could serve as benchmarks for future work.

## Conclusions

The use of  $\text{Ag}_2\text{Te}$  nanocrystals instead of  $\text{PbTe}$  nanocrystals allows for conductive coatings to be made on nylon fibre mesh without the need for high temperature ( $T > 150 \text{ }^\circ\text{C}$ ) annealing. Still, both low-temperature annealing and air plasma treatment are shown to improve the electrical

properties of  $\text{Ag}_2\text{Te}$  nanocrystal coated nylon as compared with untreated material. A prototype thermoelectric device made using the annealed and air plasma treated  $\text{Ag}_2\text{Te}$  nanocrystal coated nylon is moderately flexible and its high ( $>10 \text{ k}\Omega$ ) resistance leads to a relatively low power output of just under 0.8 nW in a 20 K temperature difference. By replacing the annealed  $\text{Ag}_2\text{Te}$  nanocrystal coating with PEDOT:PSS, the flexibility of the coated nylon device is greatly improved and the power output in a 20 K temperature difference is over 5 nW. This research highlights the key role that nanocrystal coated fibres could play as the n-type legs of flexible thermoelectric devices, while polymers and polymer composites are presently the clear choice for the p-type legs. Furthermore, the research presents a key step forward towards the direct fabrication of polymer fibre-based thermoelectric devices that can be mass produced in a fully automatic reel-to-reel manner and that can operate at or near room temperature. Future improvement is likely to be made by investigating new p-type materials with high electrical conductivity.

## Notes and references

<sup>a</sup> School of Chemical Engineering, Purdue University, West Lafayette, Indiana, 47907, USA.

<sup>b</sup> School of Physics and Optoelectronic Engineering, Dalian University of Technology, Dalian, Liaoning, 116024, China.

<sup>c</sup> Department of Chemical and Biological Engineering, Iowa State University, Ames, Iowa 50011, USA. E-mail: yuewu@iastate.edu

Electronic Supplementary Information (ESI) available: Sheet resistance of  $\text{Ag}_2\text{Te}$  nanocrystal coated nylon fibre mesh made using nanocrystals of various sizes. See DOI: 10.1039/c000000x/

This work is supported by US Air Force Office of Scientific Research (Award Number FA9550-12-1-0061).

1. L. E. Bell, *Science*, 2008, **321**, 1457–1461.
2. A. F. Joffe, *Sci. Am.*, 1958, **199**, 31–37.
3. G. J. Snyder, *Interface*, 2008, **17**, 54–56.
4. H. J. Goldsmid, *Applications of Thermoelectricity*, John Wiley & Sons, Inc., New York, 1960.
5. R. Carlton, *IEEE Trans. Veh. Commun.*, 1966, **15**, 49–53.
6. C. B. Vining, *Nat. Mater.*, 2009, **8**, 83–85.
7. T. Starmer, *IBM Syst. J.*, 1996, **35**, 618–629.
8. V. Leonov and R. J. M. Vullers, *J. Electron. Mater.*, 2009, **38**, 1491–1498.
9. H. G. Mond and G. Freitag, *Pacing Clin. Electrophysiol.*, 2014, **37**, 1728–1745.
10. K. C. See, J. P. Feser, C. E. Chen, A. Majumdar, J. J. Urban, and R. A. Segalman, *Nano Lett.*, 2010, **10**, 4664–4667.
11. S. K. Yee, N. E. Coates, A. Majumdar, J. J. Urban, and R. A. Segalman, *Phys. Chem. Chem. Phys.*, 2013, **15**, 4024–4032.
12. N. E. Coates, S. K. Yee, B. McCulloch, K. C. See, A. Majumdar, R. A. Segalman, and J. J. Urban, *Adv. Mater.*, 2013, **25**, 1629–2633.
13. M. He, J. Ge, Z. Lin, X. Feng, X. Wang, H. Lu, Y. Yang, and F. Qiu, *Energy Environ. Sci.*, 2012, **5**, 8351–8358.
14. B. Zhang, J. Sun, H. E. Katz, F. Fang, and R. L. Opila, *ACS Appl. Mater. Interfaces*, 2010, **2**, 3170–3178.

15. K. Kato, Y. Hatasako, M. Uchino, Y. Nakata, Y. Suzuki, T. Hayakawa, C. Adachi, and K. Miyazaki, *Adv. Mater. Interfaces*, 2014, **1**, 1300015.
16. Y. Yang, Z.-H. Lin, T. Hou, F. Zhang, and Z. L. Wang, *Nano Res.*, 2012, **5**, 888–895.
17. J. Chen, X. Gui, Z. Wang, Z. Li, R. Xiang, K. Wang, D. Wu, X. Xia, Y. Zhou, Q. Wang, Z. Tang, and L. Chen, *ACS Appl. Mater. Interfaces*, 2011, **4**, 81–86.
18. C. Meng, C. Liu, and S. Fan, *Adv. Mater.*, 2010, **22**, 535–539.
19. C. A. Hewitt, A. B. Kaiser, S. Roth, M. Craps, R. Czerw, and D. L. Carroll, *Appl. Phys. Lett.*, 2011, **98**, 183110.
20. J. Liu, J. Sun, and L. Gao, *Nanoscale*, 2011, **3**, 3616–3619.
21. C. Yu, Y. S. Kim, D. Kim, and J. C. Grunlan, *Nano Lett.*, 2008, **8**, 4428–4432.
22. Q. Yao, L. Chen, W. Zhang, S. Liufu, and X. Chen, *ACS Nano*, 2010, **4**, 2445–2451.
23. D. Kim, Y. Kim, K. Choi, J. Grunlan, and C. Yu, *ACS Nano*, 2010, **4**, 513–523.
24. C. Yu, K. Choi, L. Yin, and J. C. Grunlan, *ACS Nano*, 2011, **5**, 7885–7892.
25. C. Bounioux, P. Diaz-Chao, M. Campoy-Quiles, M. S. Martín-González, A. R. Goñi, R. Yerushalmi-Rozen, and C. Müller, *Energy Environ. Sci.*, 2013, **6**, 918–925.
26. G. P. Moriarty, K. Briggs, B. Stevens, C. Yu, and J. C. Grunlan, *Energy Technol.*, 2013, **1**, 265–272.
27. B. Abad, I. Alda, P. Díaz-Chao, H. Kawakami, A. Almarza, D. Amantia, D. Gutierrez, L. Aubouy, and M. Martín-González, *J. Mater. Chem. A*, 2013, **1**, 10450–10457.
28. L. Wang, Q. Yao, H. Bi, F. Huang, Q. Wang, and L. Chen, *J. Mater. Chem. A*, 2014, **2**, 11107–11113.
29. D. Liang, H. Yang, S. W. Finefrock, and Y. Wu, *Nano Lett.*, 2012, **12**, 2140–2145.
30. S. J. Kim, J. H. We, and B. J. Cho, *Energy Environ. Sci.*, 2014, **7**, 1959–1965.
31. X. Zhu, S. W. Finefrock, and Y. Wu, *The Summer Undergraduate Research Fellowship (SURF) Symposium*, 2014, Paper 73.
32. K. Suemori, S. Hoshino, and T. Kamata, *Appl. Phys. Lett.*, 2013, **103**, 153902.
33. C. Yu, A. Murali, K. Choi, and Y. Ryu, *Energy Environ. Sci.*, 2012, **5**, 9481–9486.
34. C. A. Hewitt, A. B. Kaiser, S. Roth, M. Craps, R. Czerw, and D. L. Carroll, *Nano Lett.*, 2012, **12**, 1307–1310.
35. H. Fang, Z. Luo, H. Yang, and Y. Wu, *Nano Lett.*, 2014, **14**, 1153–1157.
36. D. Cadavid, M. Ibáñez, S. Gorsse, A. M. López, A. Cirera, J. R. Morante, and A. Cabot, *J. Nanoparticle Res.*, 2012, **14**, 1328.
37. Y.-W. Liu, D.-K. Ko, S. J. Oh, T. R. Gordan, V. Doan-Nguyen, T. Paik, Y. Kang, X. Ye, L. Jin, C. R. Kagan, and C. B. Murray, *Chem. Mater.*, 2011, **23**, 4657–4659.
38. D.-K. Ko, J. J. Urban, and C. B. Murray, *Nano Lett.*, 2010, **10**, 1842–1847.
39. J. J. Urban, D. V Talapin, E. V Shevchenko, C. R. Kagan, and C. B. Murray, *Nat. Mater.*, 2007, **6**, 115–121.
40. P. F. Taylor and C. Wood, *J. Appl. Phys.*, 1961, **32**, 1–3.
41. Y. Pei, N. A. Heinz, and G. J. Snyder, *J. Mater. Chem.*, 2011, **21**, 18256–18260.
42. Y. Sun, X. Wang, and Y. Wu, unpublished.
43. H. Yang, J.-H. Bahk, T. Day, A. M. S. Mohammed, B. Min, G. J. Snyder, A. Shakouri, and Y. Wu, *Nano Lett.*, 2014, **14**, 5398–5404.
44. J. J. Urban, D. V Talapin, E. V Shevchenko, and C. B. Murray, *J. Am. Chem. Soc.*, 2006, **128**, 3248–3255.
45. Y. Tsunoda, T. Sameshima, and S. Higashi, *Jpn. J. Appl. Phys.*, 2000, **39**, 1656–1659.
46. M. Liu and H. K. Kim, *Appl. Phys. Lett.*, 2004, **84**, 173–175.
47. S. Kim, H.-J. Kim, H. R. Lee, J.-H. Song, S. N. Yi, and D. H. Ha, *J. Phys. D: Appl. Phys.*, 2010, **43**, 305402.
48. Y. Liau, N. Scherer, and K. Rhodes, *J. Phys. Chem. B*, 2001, **105**, 3282–3288.
49. I. Karakaya and W. T. Thompson, *J. Phase Equilibria*, 1991, **12**, 56–63.
50. U. Cvelbar, M. Mozetic, and M. Klanjek-Gunde, *IEEE Trans. Plasma Sci.*, 2005, **33**, 236–237.
51. S. W. Finefrock, Y. Wang, J. B. Ferguson, J. V Ward, H. Fang, J. E. Pfluger, D. S. Dudis, X. Ruan, and Y. Wu, *Nano Lett.*, 2013, **13**, 5006–5012.
52. A. F. Ioffe, *Semiconductor Thermoelements and Thermoelectric Cooling*, Infosearch, London, 1957.
53. A. Diefenderfer and B. Holton, *Principles of electronic instrumentation*, Brooks/Cole, Belmont, CA, 3rd edn., 1994.
54. M. Vosgueritchian, D. J. Lipomi, and Z. Bao, *Adv. Funct. Mater.*, 2012, **22**, 421–428.
55. D. J. Lipomi, J. A. Lee, M. Vosgueritchian, B. C. Tee, J. A. Bolander, and Z. Bao, *Chem. Mater.*, 2012, **24**, 373–382.
56. Y. Nonoguchi, K. Ohashi, R. Kanazawa, K. Ashiba, K. Hata, T. Nakagawa, C. Adachi, T. Tanase, and T. Kawai, *Sci. Rep.*, 2013, **3**, 3344.